Article

Folding of 8-17 Deoxyribozyme Studied by Three-Color Alternating-Laser Excitation of Single Molecules

Nam Ki Lee, Hye Ran Koh, Kyu Young Han, and Seong Keun Kim

J. Am. Chem. Soc., **2007**, 129 (50), 15526-15534 • DOI: 10.1021/ja0725145

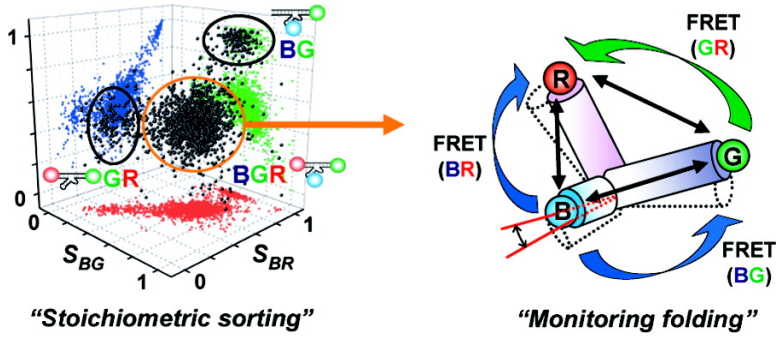

"Stoichiometric sorting" *"Monitoring folding"*

More About This Article

Additional resources and features associated with this article are available within the HTML version:

- Supporting Information
- Links to the 1 articles that cite this article, as of the time of this article download
- Access to high resolution figures
- Links to articles and content related to this article
- Copyright permission to reproduce figures and/or text from this article

View the Full Text HTML

J|A|C|S
ARTICLES
Published on Web 11/21/2007

Folding of 8-17 Deoxyribozyme Studied by Three-Color Alternating-Laser Excitation of Single Molecules

Nam Ki Lee, Hye Ran Koh, Kyu Young Han, and Seong Keun Kim*

Contribution from the School of Chemistry, Seoul National University, Seoul 151-747, Korea

Received April 11, 2007; E-mail: seongkim@snu.ac.kr

Abstract: The folding of 8-17 deoxyribozyme was investigated by three-color alternating-laser excitation (3c-ALEX), a new single-molecule fluorescence resonance energy transfer (FRET) method we recently developed. Since 3c-ALEX has the capability of simultaneously sorting fluorescent molecules based on their labeling status and monitoring three interprobe distances of a biomolecule by employing three-color FRET, it is an ideal tool to study folding of multibranched molecules. The 8-17 deoxyribozyme, a DNA enzyme that cleaves a specific RNA substrate, is a good model system for a multibranched molecule, since it has the structure of a three-way DNA junction with a bulge. Labeling all three branches of the 8-17 with different fluorescent probes, we studied its [Mg^{2+}]-dependent folding in a Na^+ buffer solution. With the stoichiometric sorting capability of 3c-ALEX, we first selected only the triply labeled 8-17 in a solution of all heterogeneous mixtures and then simultaneously measured all three interprobe distances of the selected species. Our results show that the 8-17 folds into a pyramidal form upon increasing [Mg^{2+}], in a similar way with [Zn^{2+}] as found in an earlier study conducted at the ensemble level. The apparent dissociation constant of Mg^{2+} was more than 100 times larger than that of Zn^{2+} and showed considerable variance with buffer concentration. No clear sign of two-step folding was observed for Mg^{2+}, in contrast to the case of Zn^{2+}. Compared with the hammerhead ribozyme, the 8-17 was found to require 10 times higher [Mg^{2+}] to undergo folding. By comparison with the folding of several inactive 8-17 analogues, we found that the two conserved sequences (A and G) of the triad loop of the shortest branch are critical elements for folding, especially for the folding at low [Mg^{2+}]. Our results suggest that the role of the stem loop is to provide a scaffold for the two bases to be properly positioned for the necessary interaction and that the two bases are directly involved in the interaction that plays a critical role in folding. This work demonstrates that 3c-ALEX is a powerful single-molecule method to study the structure and folding of complex and multibranched biomolecules.

Introduction

Deoxyribozyme, alternatively termed DNA enzyme, catalytic DNA, or DNAzyme, is a DNA that has the capability of performing catalytic functions as proteins and ribozymes do.[1−3] Although a deoxyribozyme has yet to be found in natural organisms, numerous *in vitro* selection studies have found that single-stranded DNA (ssDNA) shows various catalytic activities, including site-specific cleavage of RNA substrate.[4−9] Since DNA has superior chemical stability in physiological conditions over protein and RNA and is much easier to handle, deoxyribozyme has been explored with great interest for various biotechnological applications, including rapid RNA preparation,[10] metal ion sensors,[11−13] logic gates,[14,15] DNA nanomotors,[16] and also as potential therapeutic agents.[17,18]

Among deoxyribozymes, the 8-17 deoxyribozyme is the most frequently found catalytic motif by *in vitro* selection (Figure 1A),[3,6] and thus its kinetics and sequence requirement for activity have been extensively characterized.[6,8,19−23] In contrast, no study has been carried out so far on its folding, except for the initial work of Liu and Lu.[24] Consequently, current knowledge on folding of 8-17 deoxyribozyme is very limited; for instance,

(1) Sen, D.; Geyer, C. R. *Curr. Opin. Chem. Biol.* **1998**, *2*, 680−687.
(2) Emilsson, G. M.; Breaker, R. R. *Cell. Mol. Life Sci.* **2002**, *59*, 596−607.
(3) Silverman, S. K. *Nucleic Acids Res.* **2005**, *33*, 6151−6163.
(4) Breaker, R. R.; Joyce, G. F. *Chem. Biol.* **1995**, *2*, 655−660.
(5) Faulhammer, D.; Famulok, M. *Angew. Chem., Int. Ed. Engl.* **1996**, *35*, 2837−2841.
(6) Santoro, S. W.; Joyce, G. F. *Proc. Natl. Acad. Sci. U.S.A.* **1997**, *94*, 4262−4266.
(7) Geyer, C. R.; Sen, D. *Chem. Biol.* **1997**, *4*, 579−593.
(8) Li, J.; Zheng, W. C.; Kwon, A. H.; Lu, Y. *Nucleic Acids Res.* **2000**, *28*, 481−488.
(9) Feldman, A. R.; Sen, D. *J. Mol. Biol.* **2001**, *313*, 283−294.
(10) Cheong, H. K.; Hwang, E.; Lee, C.; Choi, B. S.; Cheong, C. *Nucleic Acids Res.* **2004**, *32*, e84.
(11) Li, J.; Lu, Y. *J. Am. Chem. Soc.* **2000**, *122*, 10466−10467.
(12) Liu, J. W.; Lu, Y. *J. Am. Chem. Soc.* **2003**, *125*, 6642−6643.
(13) Liu, J. W.; Lu, Y. *Anal. Chem.* **2003**, *75*, 6666−6672.
(14) Stojanovic, M. N.; Mitchell, T. E.; Stefanovic, D. *J. Am. Chem. Soc.* **2002**, *124*, 3555−3561.
(15) Stojanovic, M. N.; Semova, S.; Kolpashchikov, D.; Macdonald, J.; Morgan, C.; Stefanovic, D. *J. Am. Chem. Soc.* **2005**, *127*, 6914−6915.
(16) Chen, Y.; Wang, M. S.; Mao, C. D. *Angew. Chem., Int. Ed.* **2004**, *43*, 3554−3557.
(17) Dass, C. R. *Trends Pharmacol. Sci.* **2004**, *25*, 395−397.
(18) Takahashi, H.; Hamazaki, H.; Habu, Y.; Hayashi, M.; Abe, T.; Miyano-Kurosaki, N.; Takaku, H. *FEBS Lett.* **2004**, *560*, 69−74.
(19) Peracchi, A. *J. Biol. Chem.* **2000**, *275*, 11693−11697.
(20) Brown, A. K.; Li, J.; Pavot, C. M. B.; Lu, Y. *Biochemistry* **2003**, *42*, 7152−7161.
(21) Bonaccio, M.; Credali, A.; Peracchi, A. *Nucleic Acids Res.* **2004**, *32*, 916−925.
(22) Peracchi, A.; Bonaccio, M.; Clerici, M. *J. Mol. Biol.* **2005**, *352*, 783−794.
(23) Cruz, R. P. G.; Withers, J. B.; Li, Y. F. *Chem. Biol.* **2004**, *11*, 57−67.
(24) Liu, J. W.; Lu, Y. *J. Am. Chem. Soc.* **2002**, *124*, 15208−15216.

10.1021/ja0725145 CCC: $37.00

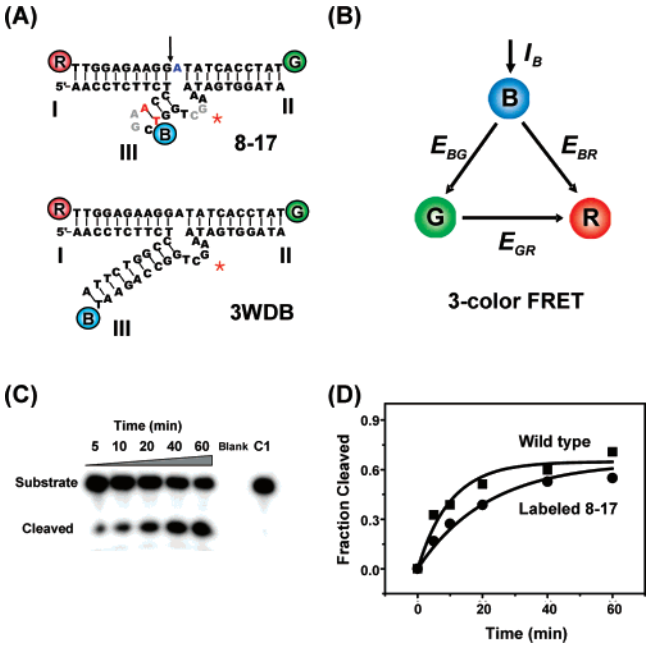

Figure 1. (A) Secondary structure and labeling scheme of 8-17 deoxyribozyme (17E)[8] and three-way DNA with a bulge (3WDB). The "bulge" is represented by a red asterisk in both cases. At stem **III**, the G−C pair of the wild type was modified to an A−T pair (red) to incorporate the fluorescent probe ***B***. Typically, the substrate for 8-17 deoxyribozyme is a DNA/RNA chimeric oligonucleotide that mostly consists of deoxyribonucleotides except for a ribonucleotide (blue) at the cleavage site (indicated by the arrow). To prevent the cleavage of the substrate, the riboadenosine was replaced by deoxyriboadenosine in the folding study. Stems **I** and **II** were, respectively, labeled by ***R*** and ***G***. The four highly conserved residues are depicted in gray.[22,23] 3WDB is prepared as an 8-17 analogue without the loop of stem **III**. (B) Scheme for three-color FRET. The excitation energy of ***B*** is transferred to ***G*** and/or to ***R***, and that of ***G***, to ***R***. FRET efficiencies E_{BG}, E_{GR}, and E_{BR} report on three interprobe distances. I_B denotes excitation of probe ***B***. (C) Activity test of the ***B***-labeled 8-17. The gel image clearly shows that the labeled 8-17 cleaves the substrate. C1: control experiment without Mg^{2+}, 1 h incubated. (D) Activity of the wild-type and the labeled 8-17. The activity of the labeled 8-17 was reduced only by 50%; k_{obs}, 0.05 min^{-1} for the labeled 8-17 and 0.10 min^{-1} for the wild-type (G-C instead of A-T in Figure 1A, red).

little is known about the folded and unfolded structures of the 8-17, the role of the divalent ions and key structural elements such as the loop and the highly conserved sequences, and the effect of monovalent ions in the buffer solution. Furthermore, the intriguing secondary structure of the 8-17 that consists of three branches of double-stranded helical arms and a bulge of single-stranded nucleotides (shown as red asterisks in Figure 1A) is quite similar to that of the well-characterized hammerhead ribozyme.[25,26] Thus it is of significant interest to compare the folding behaviors of the two catalytic nucleic acids, both of which are induced by the same or similar divalent metal ions.

To study the folding of the 8-17, three distances between each pair of the three branches have to be monitored.[24] This can be achieved by measuring fluorescence resonance energy transfer (FRET) between three fluorescent probes, often called three-color FRET (3c-FRET; Figure 1B).[24,27−31] Typically, FRET employs two fluorescent probes of a donor and an acceptor molecule; when the donor is close to the acceptor (<10 nm), the excitation energy of the donor is transferred to the acceptor via a dipole−dipole interaction. The energy transfer efficiency (E) measured reports on the distance (R) between the donor and the acceptor, since $E = 1/(1 + (R/R_o)^6)$, where R_o is a constant called the Förster radius that depends on the fluorescent probes.[32] In order to determine three distances by a typical FRET scheme that uses only two probes, one has to prepare at least three dually labeled samples and take three independent measurements to deduce three distances. By simultaneously employing three probes of different colors, however, 3c-FRET can measure all three distances at once (Figure 1B) for a triply labeled species.[28]

Recently, we developed a novel technique named three-color alternating-laser excitation (3c-ALEX) that allows one to determine multiple binding stoichiometries and measure multiple interprobe distances of biomolecules at the single molecule level.[33] The 3c-ALEX method has the capability of measuring 3c-FRET of single diffusing molecules in solution; the measured 3c-FRET not only reports on the three interprobe distances at once but also provides "virtual sorting" of molecules, i.e., identifies stoichiometrically distinct species (e.g., singly, doubly, and triply labeled samples) in a solution of heterogeneous components.[34−36] The virtual sorting is utilized to analyze the heterogeneity of the solution and select triply labeled species for quantitative 3c-FRET measurement even in the presence of a significant amount of imperfectly labeled species, which is very difficult to achieve at the ensemble level. In addition, 3c-ALEX requires no further modification of sample than fluorescent labeling, and it consumes a much smaller amount of sample (typically tens of picomolar concentration) than that required in an ensemble 3c-FRET measurement (at least tens of nanomolar concentration). These features make 3c-ALEX an ideal method to study the folding of complex molecules in solution using 3c-FRET.

In this work, we used 3c-ALEX to study the folding of a triply labeled 8-17 deoxyribozyme in solution. We used Mg^{2+} as a physiologically more relevant species to induce folding of the 8-17 than Zn^{2+} used in an earlier study[24] and compared the result with the latter as well as the Mg^{2+}-dependent folding of the hammerhead ribozyme.[37] We examined the effect of the stem loop on the folding of the 8-17 by systematically studying the folding of several 8-17 analogues. We also investigated the effect of the monovalent ion (Na^+) on folding.

Methods and Materials

Sample Preparation. We chose the sequence of 17E deoxyribozyme,[8] among the analogues of 8-17 deoxyribozyme,[20] since its kinetics and the sequence requirement for activity have been well characterized.[8,20−22] A challenge in using 3c-ALEX for folding study is to incorporate three different probe dyes at the appropriate positions of target molecules. Both the green and red fluorescent dyes ***G*** and ***R***

(25) Hammann, C.; Lilley, D. M. *ChemBioChem* **2002**, *3*, 690−700.
(26) Blount, K. E.; Uhlenbeck, O. C. *Annu. Rev. Biophys. Biomol. Struct.* **2005**, *34*, 415−440.
(27) Galperin, E.; Verkhusha, V.; Sorkin, A. *Nat. Methods* **2004**, *1*, 209−217.
(28) Watrob, H. M.; Pan, C. P.; Barkley, M. D. *J. Am. Chem. Soc.* **2003**, *125*, 7336−7343.
(29) Haustein, E.; Jahnz, M.; Schwille, P. *ChemPhysChem* **2003**, *4*, 745−748.
(30) Hohng, S.; Joo, C.; Ha, T. *Biophys. J.* **2004**, *87*, 1328−1337.
(31) Clamme, J. P.; Deniz, A. A. *ChemPhysChem* **2005**, *6*, 74−77.
(32) Clegg, R. M. *Methods Enzymol.* **1992**, *211*, 353−388.
(33) Lee, N. K.; Kapanidis, A. N.; Koh, H. R.; Korlann, Y.; Ho, S. O.; Kim, Y.; Gassman, N.; Kim, S. K.; Weiss, S. *Biophys. J.* **2007**, *92*, 303−312.
(34) Kapanidis, A. N.; Lee, N. K.; Laurence, T. A.; Doose, S.; Margeat, E.; Weiss, S. *Proc. Natl. Acad. Sci. U.S.A.* **2004**, *101*, 8936−8941.
(35) Kapanidis, A. N.; Laurence, T. A.; Lee, N. K.; Margeat, E.; Kong, X.; Weiss, S. *Acc. Chem. Res.* **2005**, *38*, 523−533.
(36) Ross, J.; Buschkamp, P.; Fetting, D.; Donnermeyer, A.; Roth, C. M.; Tinnefeld, P. *J. Phys. Chem.* B **2007**, *111*, 321−326.
(37) Bassi, G. S.; Murchie, A. I. H.; Walter, F.; Clegg, R. M.; Lilley, D. M. J. *EMBO J.* **1997**, *16*, 7481−7489.

were attached, respectively, to the T at the end of stem **I** and **II** (Figure 1A). For dual labeling, we have obtained from Operon Biotechnologies GmbH (Cologne, Germany) a substrate strand that was modified with TAMRA-dT (***G*** of this work) and Amino Modifier C6 dT at the 5′ and 3′ end, respectively. We then attached the red dye ***R*** at the 3′ end through the amino modifier group. For stem loop **III** that lacks a T in its sequence, we modified the G−C pair at the end of the stem into an A−T pair (shown in red in Figure 1A), and a blue dye ***B*** was attached to the T of this A−T pair through the amino modifier group. The effect of such modification on catalytic activity is to be verified below. In order to investigate the role of stem loop **III** in folding, we also used a three-way DNA with a bulge (3WDB; Figure 1A), with its triad loop at the stem end completely removed. For further control experiments, we also employed two other 8-17 analogues that had each of their two essential bases in the loop mutated so that their role in the folding of the 8-17 can be explicitly identified. All oligonucleotides were purchased in HPLC-purified form from Integrated DNA Technologies (Coralville, IA) or Operon Biotechnologies GmbH (Cologne, Germany) and labeled with *N*-hydroxy-succinimidyl esters of Alexa 488 (***B***) and Alexa 647 (***R***), all purchased from Molecular Probes (Eugene, OR). The labeled ssDNAs were purified by 16% polyacrylamide/5M urea gel. The labeling efficiency of each dye was >90%. Double-stranded DNAs (dsDNAs) were formed by hybridization of appropriate ssDNAs in 40 mM Tris-HCl pH 8.0, 500 mM NaCl after heating for 2 min at 95 °C and cooling to 25 °C overnight. Since 3c-ALEX provides virtual stoichiometric sorting (Figure 2),[33] we used the annealed dsDNAs in single molecule measurement without further purification. Final DNA concentration was ∼50 pM in single molecule ("SM") buffer, which consists of, unless indicated otherwise, 50 mM Tris-HCl pH 7.0, 250 mM NaCl, 100 μg/mL BSA, 1 mM mercaptoethylamine, 5% glycerol, and 0−500 mM $MgCl_2$.

Ensemble Measurement. Measurements were performed on a steady-state spectrofluorometer (QM-4/2004SE, PTI, Lawrenceville, NJ), equipped with polarization optics. We used singly labeled dsDNA in SM buffer[34] to measure the quantum yield of each dye. For TAMRA and Alexa 647, the quantum yields were 0.55 and 0.43, respectively, while, for Alexa 488, it was measured to be 0.68 and 0.95 for the 8-17 and 3WDB, respectively. We also checked for a possible change in the quantum yield of the dyes at 200 mM Mg^{2+}, at which concentration most of the folding is completed (Supporting information). For Alexa 488 and TAMRA, the quantum yield was nearly constant, whereas it was reduced by 5% for Alexa 647 at 200 mM with no further change up to 500 mM Mg^{2+}. Since a 5% reduction in quantum yield results in a decrease of only 0.01 in FRET value, which is within our measurement error, it should not affect our measurement in any significant way. The steady-state fluorescence anisotropy values of Alexa 488, TAMRA, and Alexa 647 in dsDNA were 0.07 for the 8-17 (0.10 for 3WBD), 0.19, and 0.24, respectively. The significant anisotropy values of TAMRA and Alexa 647 indicate that the fluorophores are not very freely rotating and thus may introduce a significant error in the estimation of absolute interprobe distances. For this reason, we employed the corrected FRET efficiency (*E*) rather than the interprobe distance in our folding analysis.[24]

Kinetic Assays. We tested the catalytic activity of the ***B***-labeled enzyme strand. The DNA/RNA chimeric substrate oligonucleotides (5′-TATCCACTAT[rA]GGAAGAGGTT, where rA denotes a ribonucleotide) were labeled with [γ-^{32}P]ATP using T4 polynucleotide kinase (Takara Bio, Japan). Enzyme and substrate were mixed (Tris-HCl 50 mM pH 7.0, $MgCl_2$ 10 mM, enzyme 2 μM, substrate 0.5 nM) at room temperature; the reaction was stopped at the appropriate time by adding EDTA (50 mM final concentration) and formamide (2.5 times the reaction volume, >99%). Cleaved substrates were separated from the noncleaved ones on a 20% polyacrylamide/5M urea gel. Each band was visualized by autoradiography, and the intensity of the bands was measured by image analysis software (TotalLab, NonLinear Dynamics, U.K.) (Figure 1C). We found that the modification of the sequence from G−C to A−T and the labeling of ***B*** did not affect the activity of the 8-17 much; the rate constant of cleavage for the labeled 8-17 enzyme (0.05 min^{-1}) was nearly half that for the nonlabeled wild type (0.10 min^{-1}) (Figure 1D).

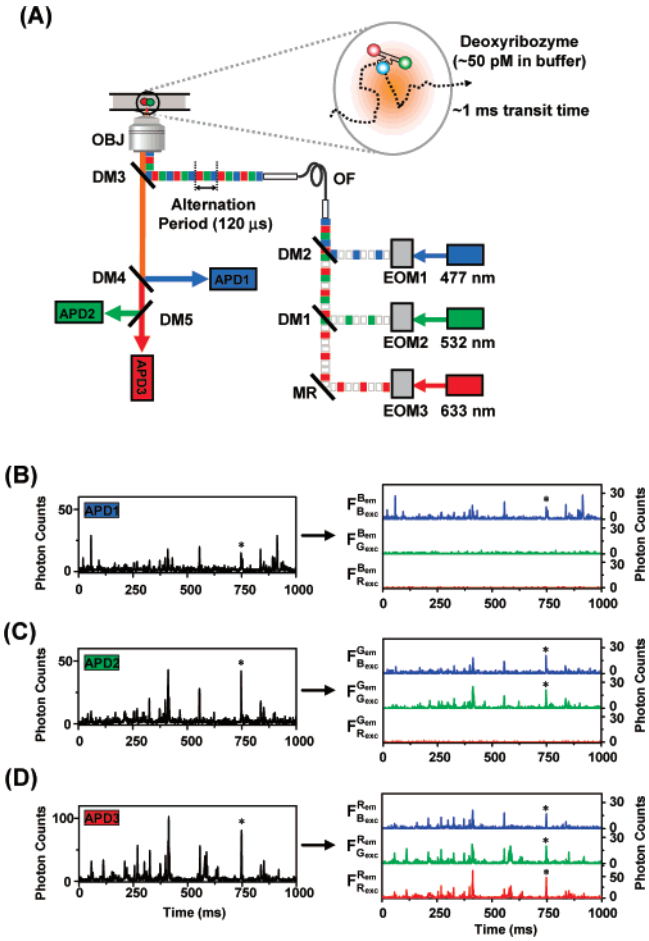

Figure 2. (A) Simplified description of the experimental setup for 3c-ALEX (OBJ, objective; DM, dichroic mirror; APD, avalanche photodiode; OF, optical fiber; MR, mirror; EOM, electro-optical modulator. For detailed explanation, see ref 33). The output of the three lasers at 477, 532, and 633 nm was modulated by three EOMs to produce a sequential pulse train of 40 μs duration and 120 μs period that excites primarily the probe ***B***, ***G***, and ***R***, respectively. Triply labeled deoxyribozymes are allowed to diffuse through the excitation volume confined by the focus of the objective (orange circle). Because of the very low concentration of the samples used (∼50 pM), usually no molecule dwells in the excitation volume; when a molecule sporadically passes through the excitation volume, it is irradiated by the lasers and allowed to emit fluorescence that appears as a burst in the time traces. (B−D) Time traces generated by 3c-ALEX with 600 μs binning. APD1 detects the emission from ***B***; APD2, emission from ***G***; and APD3, emission from ***R***. Each time trace is divided into three sub-time traces according to the excitation sources (right panel), resulting in nine photon streams. Blue, green, and red time traces originate from the 477, 532, and 633 nm excitation, respectively. Asterisks denote representatively a burst from the same molecule; the six nonzero photon counts ($F^{B_{em}}_{B_{exc}}$, $F^{G_{em}}_{B_{exc}}$, $F^{G_{em}}_{G_{exc}}$, $F^{R_{em}}_{B_{exc}}$, $F^{R_{em}}_{G_{exc}}$, and $F^{R_{em}}_{R_{exc}}$) of the burst are used to calculate three probe-stoichiometry ratio *S* and three FRET-effiency *E*.

Single-Molecule Data Acquisition and Analysis. 3c-ALEX is an extended version of 2c-ALEX that uses two alternating lasers to measure simultaneously molecular interactions (through the probe stoichiometry ratio *S*) and interprobe distances (through the FRET efficiency *E*).[34,38−40]

(38) Lee, N. K.; Kapanidis, A. N.; Wang, Y.; Michalet, X.; Mukhopadhyay, J.; Ebright, R. H.; Weiss, S. *Biophys. J.* **2005**, *88*, 2939−2953.
(39) Kapanidis, A. N.; Margeat, E.; Ho, S. O.; Kortkhonjia, E.; Weiss, S.; Ebright, R. H. *Science* **2006**, *314*, 1144−1147.
(40) Laurence, T. A.; Kong, X. X.; Jager, M.; Weiss, S. *Proc. Natl. Acad. Sci. U.S.A.* **2005**, *102*, 17348-17353.

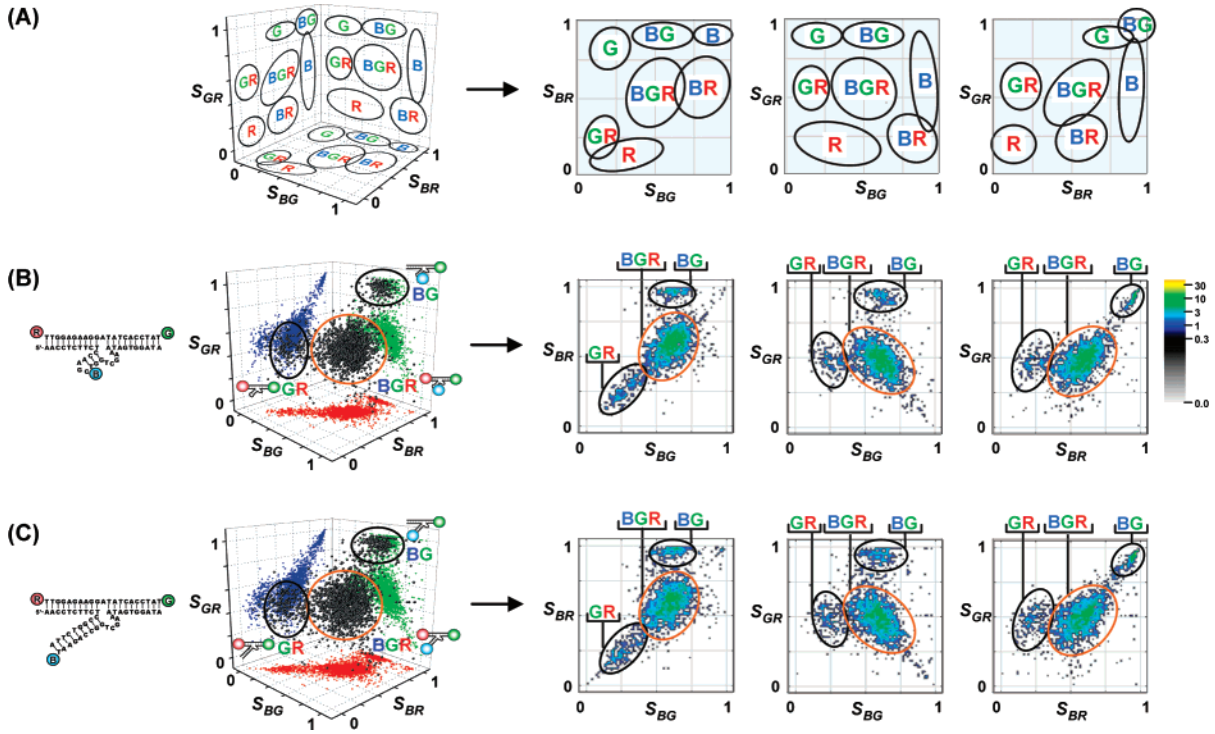

Figure 3. Virtual molecular sorting by *S* diagrams. (A) **Left**, the theoretical locations of each fluorescent species (***B***-only, ***G***-only, ***R***-only, ***B***−***G***, ***G***−***R***, ***B***−***R***, and ***B***−***G***−***R***) in three-dimensional probe-stoichiometry (3-D *S*) diagram, and **right**, its 2-D projections onto the S_{BG}-S_{BR}, S_{BG}-S_{GR}, and S_{BR}-S_{GR} planes. (B) 3-D and 2-D *S* diagrams of the solution containing 8-17 deoxyribozyme at 0 mM Mg^{2+}. Each black point in the 3-D diagram represents a single burst. The bursts for the triply labeled deoxyribozyme (***B***−***G***−***R***) can be selected (orange circle) separate from other stoichiometrically different species such as the two doubly labeled ones, ***B***−***G*** and ***G***−***R*** (indicated by black circles). (C) 3-D and 2-D *S* diagrams of the solution containing 3WDB at 0 mM Mg^{2+}.

Details of 3c-ALEX and its operating principles have been recently published,[33] and its experimental scheme is shown in Figure 2A. Here, we present a brief summary of data acquisition and analysis for 3c-ALEX.

Three lasers, each of them exciting primarily one of the three probes (Figure 1B), are modulated faster (120 μs) than the diffusion time (∼1 ms) of the sample molecule through the excitation volume (oval image in Figure 2A). The fluorescence emission from the three probes is separately detected by three detectors: APD1 for the ***B*** emission, APD2 for the ***G*** emission, and APD3 for the ***R*** emission. The fluorescence emission detected is recorded as time traces (Figure 2B−D, left panel); a fluorescent burst, here indicated representatively by an asterisk in the time traces, arises when a molecule passes through the excitation volume.[41] Each time trace is subsequently divided into three sub-time traces (shown in three different colors for each of the right panels in Figure 2B−D) based on the excitation laser source.[33] By analyzing the time traces, we select bursts (using the start/stop criterion of 18 photons per 600 μs on the sum of all time traces),[38] and each burst originating from a single diffusing molecule is characterized by nine types of photon counts (for the exact definitions, see ref 33).

The nine photon count types (Figure 2B−D, right panels) allow the calculation of three *S*'s (probe-stoichiometry ratio) and three *E**'s (proximity ratio; an analogue of FRET efficiency *E*)[41] for a burst.

Three *S*'s are calculated from

$$S_{BG} = F_{B_{exc}}/(F_{B_{exc}} + F_{G_{exc}}) \quad (1)$$

$$S_{GR} = F_{G_{exc}}/(F_{G_{exc}} + F_{R_{exc}}) \quad (2)$$

$$S_{BR} = F_{B_{exc}}/(F_{B_{exc}} + F_{R_{exc}}) \quad (3)$$

where S_{XY} refers to the probe stoichiometry specific to probes *X* and *Y*; $F_{B_{exc}}$, the sum of photon counts generated by exciting ***B*** by the 477-nm laser ($F_{B_{exc}} = F^{B_{em}}_{B_{exc}} + F^{G_{em}}_{B_{exc}} + F^{R_{em}}_{B_{exc}}$, where $F^{Y_{em}}_{X_{exc}}$ denotes the photon counts of the emission from probe *Y* upon exciting probe *X*); $F_{G_{exc}}$, sum of counts generated by exciting ***G*** by the 532-nm laser ($F_{G_{exc}} = F^{B_{em}}_{G_{exc}} + F^{G_{em}}_{G_{exc}} + F^{R_{em}}_{G_{exc}}$); and $F_{R_{exc}}$, sum of counts generated by exciting ***R*** by the 633-nm laser ($F_{R_{exc}} = F^{B_{em}}_{R_{exc}} + F^{G_{em}}_{R_{exc}} + F^{R_{em}}_{R_{exc}}$). Each species detected by all possible combinations of three colors (***B***-only, ***G***-only, ***R***-only, ***B***−***G***, ***B***−***R***, ***G***−***R***, and ***B***−***G***−***R***) has a distinct set of probe stoichiometry parameters (S_{BG}, S_{GR}, S_{BR}; Figure 3A). To maximize the discrimination power, we adjusted the relative intensity of the excitation lasers so that S_{XY} of the X−Y pair takes a value of ∼0.5. In such a case, the stoichiometric "coordinate" (S_{BG}, S_{GR}, S_{BR}) of ***B***−***R***, for example, becomes (1, 0, 0.5), while that of ***B***−***G***−***R*** becomes (0.5, 0.5, 0.5). Using this, one can identify stoichiometric distribution of all species present in solution and select a specific species in the three-dimensional *S* diagram for subsequent analysis (Figure 3).

Along with the three *S*'s, three *E**'s are calculated from

$$E^*_{BG} = F^{G_{em}}_{B_{exc}}/(F^{B_{em}}_{B_{exc}} + F^{G_{em}}_{B_{exc}}) \quad (4)$$

$$E^*_{BR} = F^{R_{em}}_{B_{exc}}/(F^{B_{em}}_{B_{exc}} + F^{R_{em}}_{B_{exc}}) \quad (5)$$

$$E^*_{GR} = F^{R_{em}}_{G_{exc}}/(F^{G_{em}}_{G_{exc}} + F^{R_{em}}_{G_{exc}}) \quad (6)$$

where E^*_{XY} stands for the proximity ratio for the *X*−*Y* pair. The three proximity ratios together with measured γ (detection efficiency correction factor;[33,38,42] Supporting information) yield three corrected FRET efficiencies (E_{BG}, E_{GR}, and E_{BR}), which in turn give three interprobe distances (R_{BG}, R_{GR}, and R_{BR}; for details, see ref 33) that are usually in the 1−10 nm range. It is to be noted that E_{BG} is a variable

(41) Deniz, A. A.; Dahan, M.; Grunwell, J. R.; Ha, T.; Faulhaber, A. E.; Chemla, D. S.; Weiss, S.; Schultz, P. G. *Proc. Natl. Acad. Sci. U.S.A.* **1999**, *96*, 3670−3675.
(42) Ha, T. J.; Ting, A. Y.; Liang, J.; Caldwell, W. B.; Deniz, A. A.; Chemla, D. S.; Schultz, P. G.; Weiss, S. *Proc. Natl. Acad. Sci. U.S.A.* **1999**, *96*, 893−898.

of only R_{BG}, independent of R_{GR} and R_{BR}. Likewise, E_{GR} and E_{BR} are dependent on only R_{GR} and R_{BR}, respectively.

Results and Discussion

Virtual Sorting of Triply Labeled 8-17 Deoxyribozyme in Heterogeneous Solution. In order to use FRET for quantitative measurement, purification of properly labeled species is a prerequisite for reliable results; the presence of a significant amount of imperfectly labeled species contaminates and thus diminishes FRET signals considerably.[32,34] Such fluorescent impurities can pose an even greater threat in the case of 3c-FRET because as many as six kinds of impurity may exist (***B***-only, ***G***-only, ***R***-only, ***B***−***G***, ***G***−***R***, and ***B***−***R***).[31,33] With the ALEX technique, however, one obtains the capability of performing "virtual sample purification" based on sample stoichiometry by using the stoichiometric parameter *S* (Figure 3A).[33] In other words, with 3c-ALEX, it is entirely possible to measure 3c-FRET quantitatively even in the presence of a considerable amount of imperfectly labeled species. This allows one to avoid the time-consuming sample purification steps such as gel purification of the triply labeled dsDNA after hybridization.

From the time traces of 8-17 deoxyribozyme solution at 0 mM Mg^{2+} (Figure 2B−D), we selected the fluorescent bursts and calculated three *S* and three *E** values of each burst. To examine the entire subpopulation distribution of the solution, three *S* values are plotted as dots in a 3-D space for all the bursts (Figure 3B, left), which can be also projected onto S_{BG}−S_{BR}, S_{BG}−S_{GR}, and S_{BR}−S_{GR} planes to yield three 2-D plots (Figure 3B, right). All *S* diagrams show three primary species clearly distinguished from one another. From the coordinates and burst counts of each species in the *S* diagrams, we identify the most abundant species in solution to be the triply labeled one (1345 counts; orange circle), while small amounts of doubly labeled species ***G***−***R*** (198 counts) and ***B***−***G*** (155 counts) are unmistakably seen to be present in solution as well. The ***B***−***R*** species is not readily seen possibly because the labeling efficiencies of ***B*** and ***R*** are significantly lower than that of ***G***, since the latter is labeled directly during the initial DNA synthesis while chemical reactions are used to label ***B*** and ***R***. We also cannot rule out the possibility of ***B*** and ***R*** being less photostable than ***G***. Figure 3C shows the *S* diagrams of 3WDB for comparison. Similar to the case of the 8-17, all three species show up, with a major component being the triply labeled species (1313 counts; ***G***−***R***, 177 counts; ***B***−***G***, 180 counts). It is clear that both solutions contain significant amounts of doubly labeled species and that such chemical heterogeneity can be fully addressed through the *S* diagrams that are obtained in 3c-ALEX.

Simultaneous Monitoring of Three Interprobe Distances. The subset of bursts selected from the *S* diagrams that correspond only to the triply labeled species (orange circle of Figure 3) can subsequently be cast into another 3-D space, spanned this time by three *E** values (Figure 4A, right). In contrast to the 3-D *S* diagram that represents stoichiometric distribution of a heterogeneous sample, the 3-D *E** diagram provides information about three interprobe distances for a stoichiometrically selected species; the mean values of E^*_{BG}, E^*_{GR}, and E^*_{BR} reflect on the distances between probe ***B*** and ***G*** (R_{BG}), ***G*** and ***R*** (R_{GR}), and ***B*** and ***R*** (R_{BR}), respectively (Figure 4A, left).[33] To determine these values, we collapsed the burst points along each axis, replotted them in three 1-D *E** diagrams (Figure 4B), and fitted each diagram with a single Gaussian function. At 0 mM Mg^{2+} (Figure 4B, top), the mean values of E^*_{BG}, E^*_{GR}, and E^*_{BR} were measured to be 0.35 ± 0.01, 0.41 ± 0.01, and 0.45 ± 0.01, respectively (black dashed line). This can be repeated for other values of Mg^{2+} concentration (Figure 4B) in an attempt to monitor the folding of the 8-17 as a function of [Mg^{2+}].

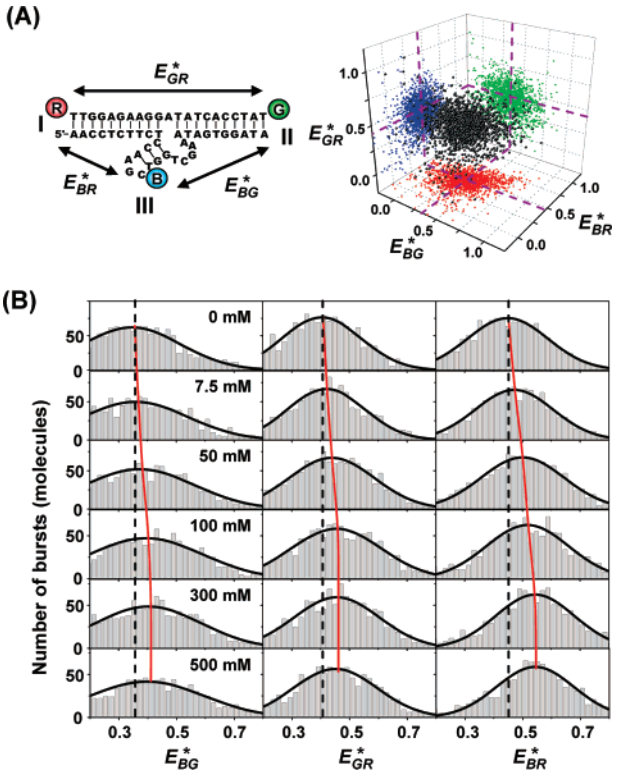

Figure 4. *E** diagrams for 8-17 deoxyribozyme. (A) 3-D *E** diagram for the triply labeled 8-17 selected from Figure 3B, orange circle. The mean values of E^*_{BG}, E^*_{GR}, and E^*_{BR} report on the distance between the probes ***B*** and ***G***, ***G*** and ***R***, and ***B*** and ***R***, respectively. (B) Three 1-D *E** diagrams of the 8-17 at various values of [Mg^{2+}]. The mean values of E^*_{BG}, E^*_{GR}, and E^*_{BR} were determined by fitting the curves to a single Gaussian function. To help better see the change, we presented *E** only in the range of 0.2−0.8. All three *E** values were seen to be gradually increased: 0.35 ± 0.01 → 0.40 ± 0.01 for E^*_{BG}, 0.41 ± 0.01 → 0.46 ± 0.01 for E^*_{GR}, and 0.45 ± 0.01 → 0.55 ± 0.01 for E^*_{BR} as [Mg^{2+}] was increased. The standard deviations were estimated from at least five independent measurements.

[Mg^{2+}]-Dependent Folding of 8-17 Deoxyribozyme. The 8-17 requires divalent metal ions for its catalytic activity[6,8] as well as for its folding.[24] Previously, Liu and Lu studied [Zn^{2+}]-dependent folding of the 8-17 by using 3c-FRET at the ensemble level.[24] They proposed that the 8-17 undergoes a two-step folding process; stem **II** of the 8-17 folds initially at 19 μM [Zn^{2+}] in such a way that reduces both angles between stems **I** and **II** and between stems **II** and **III**, and then stem **III** folds likewise to reduce both angles between stems **I** and **III** and between stems **II** and **III** at 260 μM [Zn^{2+}].

In this work, we used 3c-ALEX to investigate the folding of the 8-17 by employing a physiologically relevant divalent cation, Mg^{2+}. As shown in Figure 4B, all three *E** values gradually increased as the concentration of Mg^{2+} was increased from 0 to 500 mM: 0.35 ± 0.01 → 0.40 ± 0.01 for E^*_{BG}, 0.41 ± 0.01 → 0.46 ± 0.01 for E^*_{GR}, and 0.45 ± 0.01 → 0.55 ± 0.01 for

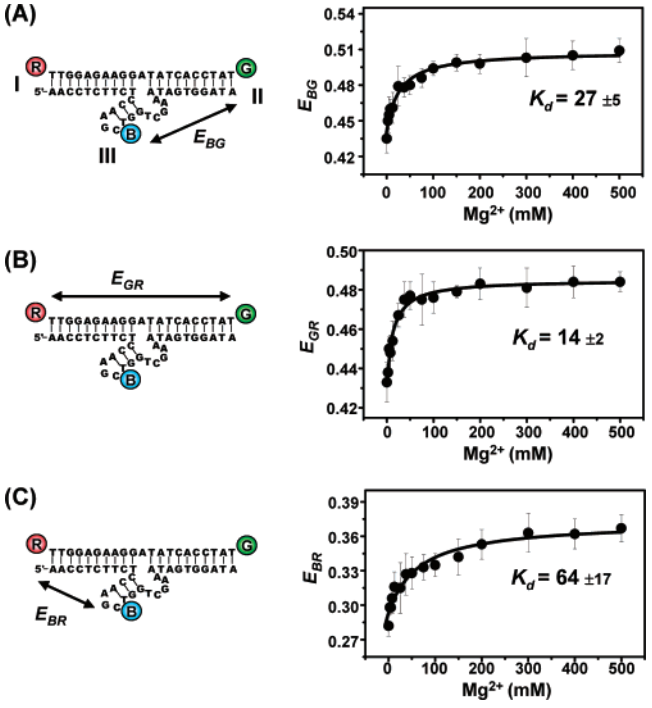

Figure 5. Folding of 8-17 deoxyribozyme. The interprobe distances are plotted as a function of [Mg^{2+}] for (A) E_{BG}, (B) E_{GR}, and (C) E_{BR}. The K_d (apparent dissociation constant) for E_{BG}, E_{GR}, and E_{BR} were measured to be 27, 14, and 64 mM, respectively. The error bar of each point was estimated from at least five independent measurements.

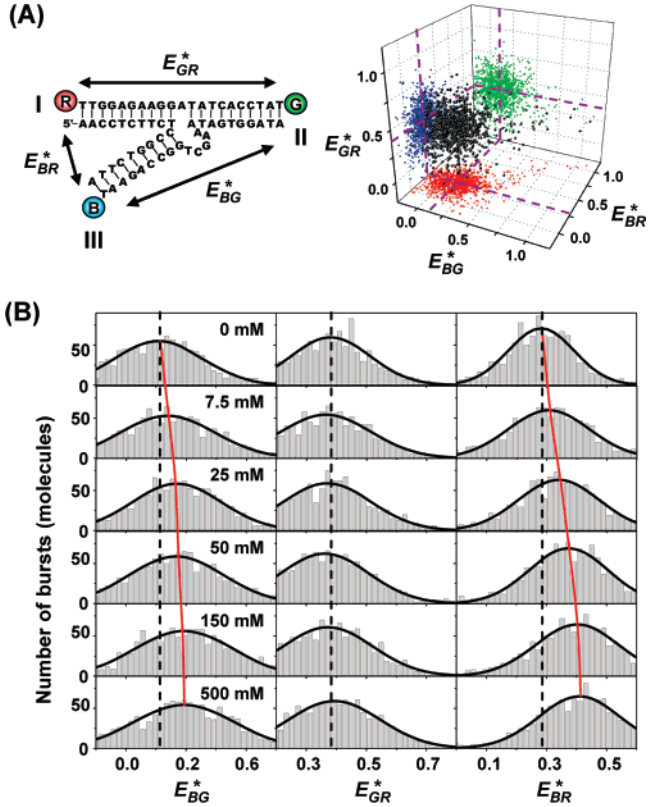

Figure 6. E^* diagrams for 3WDB. (A) 3-D E^* diagram of 3WDB selected from Figure 3C, orange circle. (B) Three 1-D E^* diagrams of 3WDB at various values of [Mg^{2+}]. Both E^*_{BG} and E^*_{BR} were seen to be gradually increased: $0.12 \pm 0.01 \rightarrow 0.20 \pm 0.01$ for E^*_{BG}, and $0.27 \pm 0.01 \rightarrow 0.40 \pm 0.01$ for E^*_{BR}, as the concentration of Mg^{2+} was increased, whereas E^*_{GR} was nearly invariant.

E^*_{BR}. The increase of all three E^* values means that all interprobe distances become shorter, as they should as the 8-17 folds into a stable conformation.

From the three E^* values measured at each Mg^{2+} concentration, we determined three corrected E values and plotted them as a function of [Mg^{2+}] in Figure 5. To obtain the apparent dissociation constant of Mg^{2+}, we fitted each graph of Figure 5 with the following equation derived from the so-called Hill plot widely used in studying ion concentration-dependent folding of RNA and DNA:[37,43]

$$E = E_i + \Delta E \cdot [Mg^{2+}]/([Mg^{2+}] + K_d) \qquad (7)$$

where E_i is the E value in the initial unfolded state, ΔE is the change in E upon addition of Mg^{2+}, and K_d is the apparent dissociation constant of Mg^{2+}. The K_d's for E_{BG}, E_{GR}, and E_{BR} were measured to be 27, 14, and 64 mM, respectively. The Hill coefficients for all three graphs were near unity: $n = 0.94$, 0.95, and 1.06 for E_{BG}, E_{BR}, and E_{GR}, respectively.

With the global folding of the 8-17 occurring at 64 mM [Mg^{2+}], the apparent dissociation constant of Mg^{2+} is at least 100 times larger than that of Zn^{2+} ($K_d = 260\ \mu$M for the second transition of the 8-17).[24] This agrees well with the order of the metal-binding affinity of the 8-17, considering the fact that the affinity of Zn^{2+} is at least 10 times higher than that of Mg^{2+}.[20]

Although the overall structural change induced by metal ion is similar between Mg^{2+} and Zn^{2+} in that all stems get closer monotonically as the 8-17 undergoes folding, the two-step nature of the folding observed with Zn^{2+} is not clearly developed in the case of Mg^{2+}. With Zn^{2+}, the two transitions are very much apart (19 vs 260 μM), with the second transition occurring at more than 10 times the Zn^{2+} concentration required for the first transition. In contrast, the folding induced by Mg^{2+} is spread over only a factor of 4 in Mg^{2+} concentration (14 to 64 mM), with an intermediate K_d value of 27 mM for E_{BG} lying between these values. Therefore it appears rather difficult to characterize the stepwise nature of the folding induced by Mg^{2+}.

Folding of 3WDB: Role of the Stem Loop in Folding of 8-17 Deoxyribozyme. It is well-known that the portion of the three base pairs in stem **III** is a solidly conserved motif among all active forms of the 8-17; a variation in the length of stem **III** reduces the activity of the 8-17 by more than 2 orders of magnitude.[20,23] In addition, two of the three bases in the end loop are also highly conserved.[22,23] It is therefore suspected that the loop of stem **III** interacts with another part of the 8-17 construct to play a significant role in its folding.[22]

To examine the effect of the loop on folding, we modified the 8-17 to 3WDB by removing the triad loop at the end of stem **III** and elongating the stem by six base pairs. With these modifications, we eliminated the possibility of interaction between the loop and the 8-17 constructs.

In much the same way as with the 8-17, we selected the bursts corresponding only to the triply labeled species from the S diagrams of Figure 3C and recast them into a 3-D E^* diagram of Figure 6A. The mean values of E^*_{BG}, E^*_{GR}, and E^*_{BR} were measured to be 0.12 ± 0.01, 0.37 ± 0.01, and 0.27 ± 0.01, respectively, at 0 mM Mg^{2+} concentration (Figure 6B, top; black dashed line). Compared with the 8-17 case in Figure 4B, both E^*_{BG} and E^*_{BR} were reduced significantly, whereas E^*_{GR} was

(43) Draper, D. E. *RNA* **2004**, *10*, 335−343.

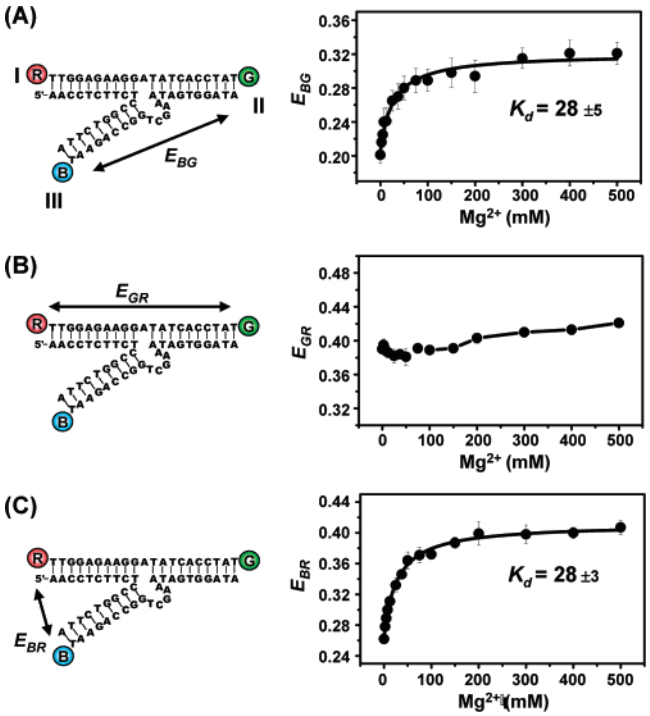

Figure 7. Folding of 3WDB. The K_d for both E_{BG} and E_{BR} were measured to be 28 mM. The K_d for E_{GR} was not measurable.

nearly invariant. This is consistent with the structural modification for 3WDB resulting from the elongation of stem **III** whose end is ***B***-labeled.

Figure 6B presents a set of 1-D E^* diagrams at various Mg^{2+} concentrations. Both E^*_{BG} and E^*_{BR} increase gradually as [Mg^{2+}] was increased: $0.12 \pm 0.01 \rightarrow 0.20 \pm 0.01$ for E^*_{BG} and $0.27 \pm 0.01 \rightarrow 0.40 \pm 0.01$ for E^*_{BR}, which is the same trend as that found for the 8-17 (Figure 4B). In contrast, however, E^*_{GR} of 3WDB shows a notably different behavior from that of the 8-17. The distance between ***G*** and ***R*** appears to change little, which is distinctly different from the monotonic decrease found in the case of the 8-17 (Figure 5B).

Figure 7 presents the same kind of results for 3WDB as Figure 5 does for the 8-17. As expected from the 1-D E^* diagrams (Figure 6B), both E_{BG} and E_{BR} increase gradually as the Mg^{2+} concentration is increased. The K_d values of E_{BG} and E_{BR} were the same at 28 mM. On the other hand, the change in E_{GR} is again small. Figure 7 apparently suggests that the expected folding of ***G*** and ***R*** at a low Mg^{2+} concentration (14 mM in the case of the 8-17) is now hindered in 3WDB because the loop of stem **III** was removed from the 8-17. Similar values of K_d for E_{BG} and E_{BR} also imply that folding of 3WDB is a one-step process where stem **III** should fold at around 28 mM [Mg^{2+}].

This result confirms that the stem-loop in 8-17 deoxyribozyme is an essential element for its catalytic activity by helping the molecule fold properly into its active form, especially by inducing the folding between stem **I** and stem **II** at a low concentration of Mg^{2+}. Such a crucial role played by the loop in folding may imply that it could possibly have a direct contact with another part of 8-17 deoxyribozyme, as mentioned earlier.[22]

Folding of Other Inactive 8-17 Analogues: Role of the Two Bases in the Conserved Sequence of the Loop. Since the two bases A and G in the loop are essential for the activity of the 8-17, it is highly likely that the loop of stem **III** interacts with another part of the 8-17 constructs through these two bases.[22,23] To further examine the role of the two conserved bases as well as the loop, we studied the folding of two 8-17 analogues, A14T and G15T, that had their A and G respectively modified to T (Figure 8). In the same way as with the 8-17 and 3WDB, we carried out 3c-ALEX measurement to obtain the interprobe distance changes of both variants as a function of [Mg^{2+}]. The results are summarized in Figure 8, which clearly shows that in both cases the folding of ***G*** and ***R*** is severely hindered, unlike in the 8-17 case. Similar values of K_d (15−19 mM [Mg^{2+}]) are also obtained for E_{BG} and E_{BR} of both analogues. These results imply that folding of both A14T and G15T is a single-step process where only stem **III** folds at around 15−19 mM [Mg^{2+}].

It is quite clear that the bases A and G of the loop are critical elements for proper folding of the 8-17, which explains why they have been highly conserved in *in vitro* selections. Furthermore, the fact that the two variants whose single base of the loop is mutated fold in a very similar way with 3WDB whose loop is completely removed strongly suggests that the stem loop plays its role in folding through A and G. There is also a significant structural difference between the variants and the 8-17; the unfolded and folded structures of A14T and G15T are nearly identical to each other (Figure 8) but considerably different from those of the 8-17 (Figure 5). We note, for example, that E_{BG} of the variants is smaller than that of the 8-17 by 0.06 whereas E_{BR} of the variants is larger by 0.14−0.17 in the unfolded state. Mutation of one of the two bases results in different structures not just in the folded state but in the unfolded state as well. Stem **III** of the variants appears to be more inclined to stem **I** than in the 8-17 in their unfolded state. This may imply that A and G of the loop are already interacting with another part of the 8-17 in the unfolded state, which can further develop during the course of folding. It is likely that these two bases are directly interacting with the 8-17 construct and that the role of the stem loop is to provide a scaffold for the two bases to be properly positioned for their interaction. Considering the secondary structure, possible candidates for such a contact site may include the core catalytic region, the single-stranded bulge, and one of the helical arms, but a further study is needed to elucidate which part of the molecule the loop interacts directly with.

Effect of Na^+ Concentration on K_d of Mg^{2+}. The apparent dissociation constants K_d for Mg^{2+} from our measurement (14−64 mM) are significantly larger than those determined from catalytic rates in other studies (10−15 mM).[20,21] Such a discrepancy could have resulted from the fact that we used a higher concentration of Na^+ (250 mM) to stabilize the dsDNA form than those in other studies (75−100 mM). All our measurements were taken at a [Na^+] of 100 mM or higher since melting of dsDNA occurs at a lower concentration of Na^+ under our experimental conditions. With a higher concentration of monovalent ions in our case, a stronger competition for divalent ions exists toward binding to the 8-17, and therefore more divalent ions are needed to induce folding.[44,45]

To examine the effect of the monovalent ion concentration on K_d of Mg^{2+} and also to estimate approximate K_d values at

(44) Uchida, T.; He, Q.; Ralston, C. Y.; Brenowitz, M.; Chance, M. R. *Biochemistry* **2002**, *41*, 5799−5806.
(45) Wilson, T. J.; Lilley, D. M. *RNA* **2002**, *8*, 587−600.

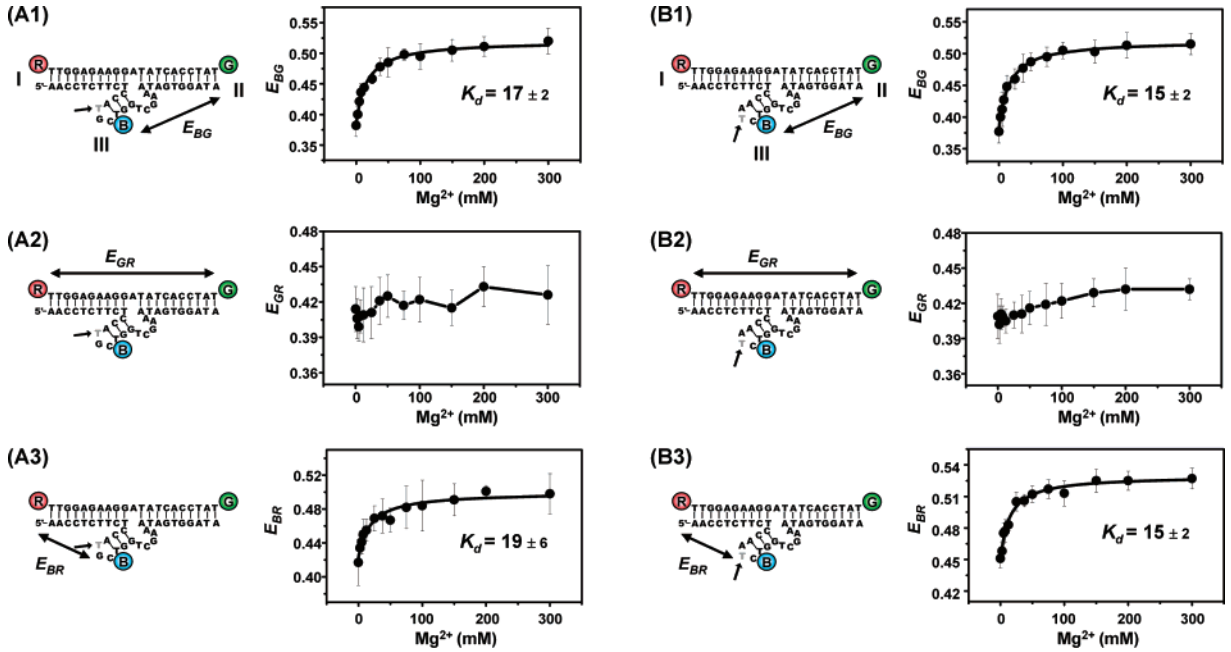

Figure 8. Folding of inactive 8-17 analogues. The corrected *E* values are plotted as a function of [Mg^{2+}] for (A1−A3) A14T and (B1−B3) G15T. Arrows indicate the positions of mutation.

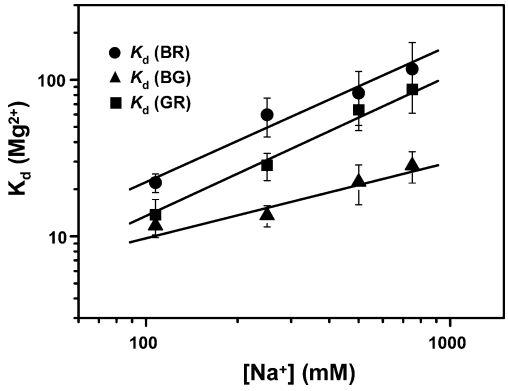

Figure 9. [Na^+]-dependent K_d of Mg^{2+}. K_d of Mg^{2+} was measured at four values of Na^+ concentration (108, 250, 500, and 750 mM). We observed that melting of the dsDNA started from 100 mM Na^+ under our experimental conditions (data not shown). The error bars were estimated from at least four independent measurements.

low Na^+ concentrations, we made a series of K_d measurements at Na^+ concentrations of 108, 500, and 750 mM (Figure 9). As expected, K_d is seen to increase as the concentration of Na^+ is increased.[44,45] To estimate the K_d value for the global folding at a Na^+ concentration of 75−100 mM,[44] we extrapolated the log−log plot of K_d(BR) and obtained 17−22 mM for K_d, which is quite comparable to the values determined from catalytic rates.[20,21]

Comparison of 8-17 Deoxyribozyme and the Hammerhead Ribozyme. The comparison between the folding of the 8-17 and hammerhead ribozyme has already been discussed before.[24] As Liu and Lu have observed, the most notable difference between the two molecules is found in their folded structures. In the case of the hammerhead ribozyme, the first transition involves coaxial stacking of two stems (stems **II** and **III**), followed by the motion of stem **I** in the second transition where it moves away from stem **III** and closer to stem **II**.[25,37] On the contrary, all stems of the 8-17 get closer to form a pyramidal structure (Figure 5).

Since we used the same divalent ion (Mg^{2+}) as the one used in the folding study of the hammerhead ribozyme,[46] we can draw two more points of difference between the two molecules. First, the 8-17 requires a 10 times higher Mg^{2+} concentration to fold than the hammerhead ribozyme does. The amount of [Mg^{2+}] needed for the second transition of the minimal hammerhead ribozyme is about 2 mM,[37] but 8-17 deoxyribozyme requires at least a 20 mM [Mg^{2+}] for its full transition (under a low [Na^+] condition). Second, the minimal hammerhead ribozyme undergoes a clear two-step folding process, whereas the 8-17 does not show a clearly defined two-step folding transition.

Conclusions

We used our newly developed 3c-ALEX technique to study the [Mg^{2+}]-dependent folding of 8-17 deoxyribozyme at the single-molecule level. The stoichiometic sorting capability of 3c-ALEX allowed us to virtually purify the triply labeled 8-17 in the presence of considerable heterogeneity in solution and subsequently measure quantitatively 3c-FRET to monitor three interprobe distances of the 8-17. Our study confirmed that the 8-17 folds to form a pyramidal structure upon adding Mg^{2+} as it does with Zn^{2+}, but the two-step transitions induced by Zn^{2+} is not clear. We also found that the loop of the shortest branch with its two highly conserved bases (A and G) plays a crucial role in the folding between stem **I** and stem **II** at a low Mg^{2+} concentration. Compared with the hammerhead ribozyme, the 8-17 needed a 10 times higher Mg^{2+} concentration for folding.

This work demonstrates that 3c-ALEX is an excellent tool for the study of complex structures and their changes at the single-molecule level, with possible applications in complex biological processes for multicomponent interactions and multistep signal transduction and ultrasensitive binding assays.

(46) Stage-Zimmermann, T. K.; Uhlenbeck, O. C. *RNA-Publ. RNA Soc.* **1998**, *4*, 875−889.

Acknowledgment. We thank Prof. Chul-hak Yang and Dr. Chi-hoon Park for their help in activity measurement. This work was funded by the National Research Laboratory Program of KOSEF and the Chemical Genomics grant of MOST as well as the Star Faculty Program of MOE, all of the Korean Government.

Supporting Information Available: Details of the changes in quantum yield of the probe dyes and detection efficiency correction factor. This material is available free of charge via the Internet at http://pubs.acs.org.

JA0725145